*International Journal of Innovative Computing, Information and Control*
Volume **21**, Number **3**, June **2025**

ICIC International ©2025 ISSN 1349-4198
pp. **649–665**

# EVENT-TRIGGERED MODEL-FREE ADAPTIVE INTEGRAL SLIDING MODE CONSTRAINED MAXIMUM POWER POINT TRACKING CONTROL STRATEGY FOR PHOTOVOLTAIC SYSTEM

Zhenchao Han[1], Tinglong Pan[1,*] and Dezhi Xu[2]

[1]School of Internet of Things Engineering
Jiangnan University
No. 1800, Lihu Avenue, Wuxi 214122, P. R. China
6221915009@stu.jiangnan.edu.cn; *Corresponding author: tlpan@jiangnan.edu.cn

[2]School of Electrical Engineering
Southeast University
No. 2, Sipailou, Xuanwu District, Nanjing 210096, P. R. China
xudezhi@seu.edu.cn

Received October 2024; revised February 2025

Abstract. *In this paper, a model-free adaptive maximum power point tracking (MPPT) control strategy is proposed to address the issues with the MPPT methods used in previous photovoltaic systems. Firstly, a nonlinear model of the photovoltaic system is established, the nonlinear model is described as an equivalent linear model through a compact form dynamic linearization method, and the pseudo partial derivative is estimated based on an observer-based adaptive law. Then, an anti-windup compensator is used to solve the actuator saturation phenomenon in the control system, and a control law is designed on the integral sliding mode surface to enhance the robustness of the system. Considering the computational pressure and cost of the actual system, an event triggering mechanism is designed, which only updates the control signal when the preset event triggering conditions are met, and the stability of the proposed control algorithm is proved. Finally, the good applicability and control performance of the proposed control strategy on photovoltaic systems are verified by simulation results.*

**Keywords:** Maximum power point tracking, Event-triggered control, Model-free adaptive control, Sliding mode constrained control

1. **Introduction.** In the past few decades, solar energy has been regarded as the most important clean energy source, and people have been continuously researching related technologies to achieve greater utilization of solar energy. Among them, photovoltaic maximum power point tracking (MPPT) technology has received much attention. When the photovoltaic cell operates at its maximum power point, the output power of the photovoltaic cell is maximized, and the highest photoelectric conversion rate can be obtained. In order to enable photovoltaic cells to operate at maximum power under different external environmental conditions, it is necessary to adopt appropriate MPPT control methods to track the maximum power point of photovoltaic cells. At present, there are many methods for MPPT, and traditional control methods include constant voltage tracking (CVT) control, perturbation and observation method (P&O) control, conductance increment (INC) control, etc. Based on this, a series of improved algorithms and hybrid algorithms have been derived [2-4]. With the continuous advancement of control technology, some intelligent control methods and optimization algorithms have also been applied to MPPT

DOI: 10.24507/ijicic.21.03.649

technology [2], such as neural network control [5], sliding mode control (SMC) [6], fuzzy control [7], model predictive control [8], and genetic algorithm [9].

Under the influence of external conditions such as light intensity and battery temperature, the output characteristics of the battery have strong randomness and fluctuation. The traditional MPPT control methods can achieve maximum power tracking, but the tracking performance is not satisfactory, especially when the environmental conditions change greatly. Taking disturbance observation as an example, the output of its controller is the voltage change signal, which needs to be combined with PID control to obtain the duty cycle signal. At this point, it is not only necessary to have a suitable step size, but also to adjust the parameters in the PID, which can result in poor control performance and difficulty in responding well to environmental changes. Fuzzy control, neural network control, and model predictive control have also been applied in MPPT control of photovoltaic systems. However, fuzzy control requires setting membership functions and control rules, neural network control requires certain data for training, and model predictive control relies on an accurate system model. It is necessary to study a photovoltaic system MPPT control strategy that has fast tracking speed, high tracking accuracy, and strong stability, can cope with external environmental changes, and does not rely on model information to address the problems of existing MPPT control methods in the past.

In 1994, Professor Hou Zhongsheng first proposed the model-free adaptive control (MFAC) method [10], which was a novel control method for discrete-time nonlinear systems at that time. MFAC is essentially a data-driven control method that, when applied to nonlinear systems, first requires equivalent dynamic linearization of the system model. The MFAC algorithm has three different dynamic linearization data models, which are suitable for systems with different numbers of inputs and outputs. Specifically, the compact format dynamic linearization (CFDL) model is suitable for single input single output systems, the partial format dynamic linearization model is suitable for multiple input and single output systems, and the full format dynamic linearization model is suitable for complex multiple input and multiple output systems [11]. Compared to the other two models, the model of CFDL technology is simpler and has similar control performance. The MFAC algorithm only requires the input and output data of the controlled system, without relying on the mathematical model of the system, and has strong applicability in practical systems [12].

At present, most MFAC algorithms continuously update control signals, which may sacrifice computational costs to seek better performance. In order to reduce computational burden, scholars have explored the combination of MFAC and event-triggered control (ETC). In recent years, ETC has received increasing attention. Unlike traditional sampling control, ETC controllers are used, and the control signal is only updated when a specific "event" is triggered, which is bound to effectively save computing resources. In 1999, Professor Åarzén proposed the concept of event triggering and combined it with PID control, which proved the effectiveness of ETC [13]. At present, research in related areas is still ongoing [10,14-17]. These studies indicate that the control strategy combining ETC and MFAC is feasible.

This article introduces an event-triggered model-free adaptive integral sliding mode constrained control method into photovoltaic systems to achieve maximum power tracking control. By introducing an anti windup compensator into the proposed integral sliding mode constrained control strategy to solve the actuator saturation problem, the robustness and performance of the control system are ensured. Meanwhile, an event triggering mechanism is proposed and integrated into the proposed control strategy. Unlike traditional MFAC algorithms that calculate control signals at fixed sampling times, the proposed algorithm only updates the control signal when the event triggering parameters meet the

design conditions. In addition, the event triggering mechanism and event triggering parameters proposed in this article are designed based on the system output data; therefore, the control performance and computational cost of the system output can be balanced by adjusting the preset event triggering parameters.

The rest of this article is organized as follows. In Section 2, based on the output characteristics of photovoltaic cells and the circuit structure adopted by the photovoltaic system, a nonlinear model of the photovoltaic system is constructed. A data-driven model of the nonlinear photovoltaic system is established through a compact form of dynamic linearization method and an observer based pseudo partial derivative (PPD) estimation algorithm. Then, in Section 3, an integrated sliding mode constrained control strategy for photovoltaic systems is proposed, which is combined with event-triggered mechanisms and analyzed for its stability. Afterwards, the proposed control method is subjected to simulation experiments in Section 4 to verify its feasibility. Finally, Section 5 presents some conclusions drawn from the research.

## 2. **Preliminaries.**

### 2.1. **Nonlinear model of photovoltaic system.**

Figure 1 shows the $P$-$U$ characteristic curve of a photovoltaic cell. According to the analysis of the traditional incremental conductance method [2], the condition for the photovoltaic cell to operate at the maximum power point is the derivative of power with respect to voltage $dP/dU = 0$, and $P = U \cdot I$. Therefore, it can be concluded that

$$\frac{I}{U} + \frac{dI}{dU} = 0 \tag{1}$$

That is, at the maximum power point, the sum of the instantaneous rate of change of conductance and conductance is zero. Let it be $Y$, that is,

$$Y = \frac{I}{U} + \frac{dI}{dU} \tag{2}$$

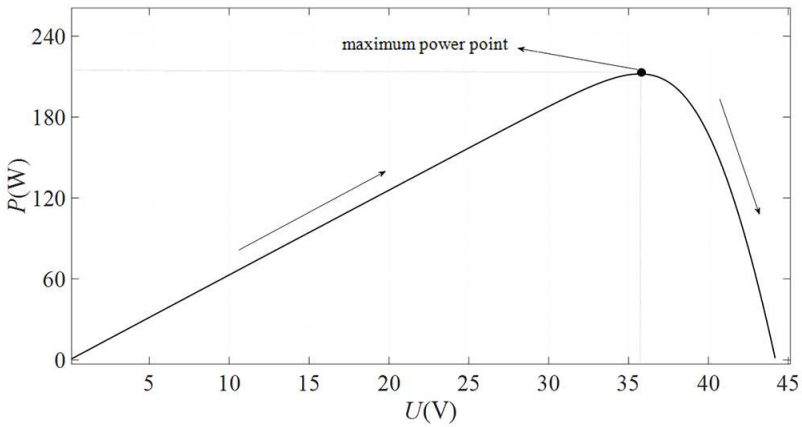


FIGURE 1. $P$-$U$ characteristic curve of photovoltaic cell

According to the expression of battery output current in [18] and the relationship between output voltage and input voltage in Boost circuit [19], the specific expression of $Y(k)$ can be obtained as follows:

$$Y(k) = \frac{I_{sc}}{(1 - D(k))U_{out}}(1 + K_1) - I_{sc} \cdot K_1 \left( \frac{1}{(1 - D(k))U_{out}} + \frac{1}{K_2 U_{oc}} \right) \mathrm{e}^{\frac{(1-D(k))U_{out}}{K_2 U_{oc}}} \tag{3}$$

where $k$ represents the current operating time of the system, $D(k)$ is the duty cycle, $U_{out}$ is the output voltage of the Boost circuit, $I_{sc}$ and $U_{oc}$ are the short-circuit current and open circuit voltage of the photovoltaic cell, and $K_1$ and $K_2$ are two undetermined coefficients. The specific expressions are shown in [18].

In the subsequent equivalent linearization and controller design, Equation (3) will be used as the nonlinear model of the photovoltaic system. It can be seen that there is a strong nonlinear relationship between $Y(k)$ and the duty cycle $D(k)$. However, the complex nonlinear relationships result in poor control performance of model-based methods. Therefore, the MFAC method is used to achieve maximum power point tracking of photovoltaic systems in this paper.

2.2. **Observer based PPD estimation algorithm.** The model (3) of the photovoltaic system can be regarded as a single input and single output system, so the CFDL method is adopted to linearize it equivalently in this paper. Model (3) is rewritten in the following general form:

$$Y(k+1) = f(Y(k), \ldots, Y(k-n_Y), D(k), \ldots, D(k-n_D)) \tag{4}$$

where $Y(k) \in R$ and $D(k) \in R$ respectively represent the output and input signals of the photovoltaic system at time $k$, $n_Y$ and $n_D$ are two positive integers representing unknown output and input sequences, and $f(\cdot)$ is an unknown nonlinear function.

For photovoltaic system (3), when $|\Delta D(k)| \neq 0$ holds, there must be a PPD parameter $\phi(k)$ that allows the model of the photovoltaic system (3) to be converted into the following equivalent CFDL model [10]:

$$\Delta Y(k+1) = \phi(k)\Delta D(k) \tag{5}$$

Since the value of PPD cannot be directly obtained from the system, an observer based estimation algorithm is used to estimate the value of PPD online in this paper [11]. Firstly, provide the structure of the output observer as follows:

$$\hat{Y}(k+1) = \hat{Y}(k) + \hat{\phi}(k)\Delta D(k) + G_o e_o(k) \tag{6}$$

where $\hat{Y}(k)$ is the estimated value of the system output, $\hat{\phi}(k)$ is the estimated value of PPD, $G_o$ is the undefined observer gain, and $e_o(k) = Y(k) - \hat{Y}(k)$ represents the estimation error of the system output.

The dynamic characteristics of the output estimation error can be obtained by combining Equations (5) and (6) as follows:

$$e_o(k+1) = \alpha e_o(k) + \varphi(k)\Delta D(k) \tag{7}$$

where $\alpha = 1 - G_o$ is the coefficient of output observation error, with a value range of $-1 < \alpha < 1$, and $\varphi(k) = \phi(k) - \hat{\phi}(k)$ represents the estimation error of PPD.

On the basis of the above content, the update law of PPD estimation value is defined as

$$\hat{\phi}(k+1) = \hat{\phi}(k) + G_1(k)\Delta D(k)(e_o(k+1) - \alpha e_o(k)) \tag{8}$$

where $G_1(k) = 2\big(\beta + \Delta D^2(k)\big)^{-1}$, and $\beta$ is a positive constant that limits the variation of PPD.

Considering that $D(k)$ is bounded, then $\Delta D(k)$ is also bounded. Assuming $|\Delta D(k)| \leq d_1$, then $G_1(k)$ satisfies

$$G_1(k) \geq \frac{2}{d_1^2 + \beta} = d_2 \tag{9}$$

In addition, from Equations (7) and (8), and considering $\Delta\phi(k) \approx 0$, the dynamic characteristics of $\varphi(k)$ can be derived as follows:

$$\varphi(k+1) = G_2(k)\varphi(k) \tag{10}$$

where $G_2(k) = 1 - G_1(k)\Delta D^2(k)$ represents the gain of $\varphi(k)$. According to Equation (9), $G_2(k) < 1$ can be obtained.

To ensure the tracking ability of PPD for time-varying parameters, a PPD reset mechanism is defined as follows [10]:

$$\hat{\phi}(k) = \hat{\phi}(1), \text{ if } \left|\hat{\phi}(k)\right| \leq \sigma \text{ or } |\Delta D(k)| \leq \sigma \text{ or } \text{sign}\left(\hat{\phi}(k)\right) \neq \text{sign}\left(\hat{\phi}(1)\right) \tag{11}$$

where $\sigma$ is a positive constant, sign$(\cdot)$ is the sign function, and $\hat{\phi}(1)$ is the initial value of $\hat{\phi}(k)$.

Considering the structure of the output observer in Equation (6), the output of the system at time $k+1$ can be expressed as

$$Y(k+1) = \hat{Y}(k) + \hat{\phi}(k)\Delta D(k) + G_o e_o(k) + e_o(k+1) \tag{12}$$

Due to the inability to obtain the value of $e_o(k+1)$ at the $k$ moment, a two-step delay estimation algorithm is used to estimate $e_o(k+1)$ in this paper, as shown below [20]:

$$e_o(k+1) \approx 2e_o(k) - e_o(k-1) \tag{13}$$

By substituting it into Equation (12), the output of the system can be further expressed as

$$Y(k+1) = \hat{Y}(k) + \hat{\phi}(k)\Delta D(k) + (2 + G_o)e_o(k) - e_o(k-1) \tag{14}$$

At this point, the CFDL linearization process and observer based PPD estimation algorithm design have been completed, and the processing of the photovoltaic power generation system model has been completed, laying the foundation for the subsequent controller design.

## 3. Controller Design.

### 3.1. Design of model-free adaptive integral sliding mode constrained MPPT controller.

Sliding mode control has strong robustness and is not affected by system parameter changes and external disturbances, and has been widely used in various industrial systems [6]. Given the above advantages, integral sliding mode control (ISMC) is introduced in this paper. In this section, based on the previous section, a model-free adaptive integral sliding mode constrained control algorithm is further designed. Firstly, the tracking error output of the system is defined as

$$e(k) = Y^*(k) - Y(k) - \theta(k) \tag{15}$$

where $Y^*(k)$ represents the reference signal output by the system, and $\theta(k)$ is the compensation signal.

Due to factors such as algorithm or performance, the actuator may experience saturation during signal conversion. The saturation problem reduces the stability of the system and causes certain power losses. Therefore, this article introduces an anti-windup compensator into the MPPT control system, which simulates actuator saturation by imposing constraints on $D(k)$, thereby compensating for the loss of output signals and ensuring the stability of photovoltaic system operation [20]. In a photovoltaic power generation system, the system input is the duty cycle $D(k)$. According to its definition, $D(k)$ is only constrained by amplitude, as shown below:

$$D_{\max} > D(k) > D_{\min} \tag{16}$$

where $D_{\max}$ and $D_{\min}$ respectively represent the maximum and minimum values of $D(k)$, and both are constants. According to the actual physical meaning of the duty cycle, it can be inferred that $0 \leq D_{\min} < D_{\max} \leq 1$.

According to Equation (16), the constrained $D(k)$ can be expressed as

$$D(k) = \text{Sat}\left\{D_o(k), D_{\max}, D_{\min}\right\} \tag{17}$$

where $D_o(k)$ represents the duty cycle before applying the limiting constraint, and its definition will be given later. $\text{Sat}(\cdot)$ is a limiting function.

According to the amplitude constraint on $D(k)$, the dynamic characteristics of $\theta(k)$ are defined as

$$\theta(k+1) = \eta\theta(k) + \hat{\phi}(k)(D_o(k) - D(k)) \tag{18}$$

where $\eta$ is the gain coefficient of $\theta(k)$, with a value range of $(0, 1)$.

Next, based on the error $e(k)$, the design of the integral sliding mode surface [20] is carried out as follows:

$$s(k) = e(k) + \lambda \sum_{i=1}^{k} T_s e(i) \tag{19}$$

where $\lambda > 0$, $T_s > 0$ is the system sampling periods.

Due to the fact that sliding mode control includes two stages, namely the arrival stage and the sliding stage, it is necessary to design control laws for each stage separately. In order to ensure system stability, it is necessary to operate the system state on the sliding surface as much as possible and ultimately reach the equilibrium point. Therefore, this article focuses on the sliding phase and adopts an equivalent control law to limit the system state, keeping it on the sliding surface. The equivalent control law is as follows:

$$\begin{aligned} D_{eq}(k) = \frac{\hat{\phi}(k)}{\hat{\phi}^2(k) + \varepsilon} \Bigg( \left( \frac{1}{\lambda T_s + 1} - \eta \right) \theta(k) + e_o(k-1) - (2 + G_o) e_o(k) \\ + \frac{Y(k)}{\lambda T_s + 1} - \hat{Y}(k) \Bigg) \end{aligned} \tag{20}$$

where $\varepsilon$ is a sufficiently small positive constant.

For the arrival stage, a switching control law is adopted. This control law can make the system state that deviates far from the sliding surface return to the sliding surface again, thereby ensuring control performance. The switching control law is as follows:

$$D_{sw}(k) = \frac{\hat{\phi}(k)}{\hat{\phi}^2(k) + \varepsilon} \cdot \frac{\upsilon \text{sign}(s(k)) + \mu s(k)}{1 + \lambda T_s} \tag{21}$$

where $\upsilon > 0$ is the switching coefficient, and $0 < \mu < 2$ is the convergence coefficient.

Combining the equivalent control law with the switching control law, the following expression for $D_o(k)$ is given:

$$D_o(k) = D(k-1) + D_{eq}(k) + D_{sw}(k) \tag{22}$$

Combining Equation (17), the structure of the model-free adaptive sliding mode constrained MPPT controller can be obtained as follows:

$$\begin{cases} D_o(k) = D(k-1) + D_{eq}(k) + D_{sw}(k) \\ D(k) = \text{Sat}\left\{D_o(k), D_{\min}, D_{\max}\right\} \end{cases} \tag{23}$$

3.2. **Controller design based on event triggering.** This section uses the actual tracking error output of the system to design the event triggering mechanism. And the actual tracking error $E(k)$ of the system is defined as follows.

$$E(k) = Y(k) - Y^*(k) \tag{24}$$

Next, based on $E(k)$, define the following event triggering error $e^{ET}(k)$:

$$e^{ET}(k) = E(k) - E(k_i), \quad k_i \leq k < k_{i+1} \tag{25}$$

where $k_i$, $i = 1, 2, 3, \ldots$ is the event triggering time, and $E(k_i)$ represents the actual tracking error of the MPPT control event triggering time before and closest to the current time $k$.

Finally, based on the output voltage of the photovoltaic cell and whether it is near the maximum power point, as well as the event triggering error $e^{ET}(k)$ mentioned above, the following event triggering conditions are set.

When the system starts running, if the event triggering error $e^{ET}(k)$ is within a certain range, the first layer event is triggered. When $\left|e^{ET}(k)\right| \geq \delta$ is applied, MPPT control is applied, where $\delta \geq 0$ is the threshold for event triggering error; When the system power approaches the maximum power point, that is, when the absolute value of $Y = dP/dU$ is less than a certain value $\rho$, the second layer event is triggered. At this point, select a threshold with a larger event triggering error to further reduce the number of control iterations and lower control costs. In this article, $\delta$ and $\rho$ are both referred to as event-triggered parameters.

After being combined with ETC, the PPD estimation algorithm and integral sliding mode control algorithm will only run at the event triggering moment. Therefore, the structure of the event-triggered model-free adaptive integral sliding mode constrained MPPT controller can be obtained as follows:

$$\begin{cases} D_o(k) = \begin{cases} D(k-1) + D_{eq}(k_i) + D_{sw}(k_i), & k = k_i \\ D(k-1), & k \in (k_i, k_{i+1}) \end{cases} \\ D(k) = \mathrm{Sat}\left\{D_o(k), D_{\min}, D_{\max}\right\} \end{cases} \tag{26}$$

During the time when the event is not triggered, the duty cycle remains unchanged, i.e., $\Delta D(k) = 0$. Considering the PPD reset mechanism Equation (11), the update law for event-triggered PPD estimation values is as follows:

$$\hat{\phi}(k+1) = \begin{cases} \hat{\phi}(k) + G_1(k_i)\Delta D(k_i)(e_o(k_i{+}1) - \alpha e_o(k_i)), & k = k_i \\ \hat{\phi}(1), & k \in (k_i, k_{i+1}) \end{cases} \tag{27}$$

Finally, the above event-triggered MFAC control strategy diagram is shown in Figure 2.

### 3.3. **Stability proof.**

**Theorem 3.1.** *For the photovoltaic system model (3), under the proposed model-free adaptive integral sliding mode constrained MPPT controller, by selecting appropriate parameters, it is possible to ensure that the defined system output tracking error $e(k)$ satisfies the final uniform boundedness, that is,*

$$\lim_{k\to\infty} |e(k)| = 0 \tag{28}$$

**Proof:** By defining the Lyapunov function as $V(k) = \frac{1}{2}s^2(k)$, we can obtain

$$\begin{aligned} \Delta V(k+1) &= V(k+1) - V(k) \\ &= \frac{1}{2}s^2(k+1) - \frac{1}{2}s^2(k) \\ &= \frac{1}{2}(s(k+1) - s(k))(s(k+1) + s(k)) \end{aligned}$$

$$= \Delta s(k+1)\left[\frac{1}{2}\Delta s(k+1) + s(k)\right] \tag{29}$$

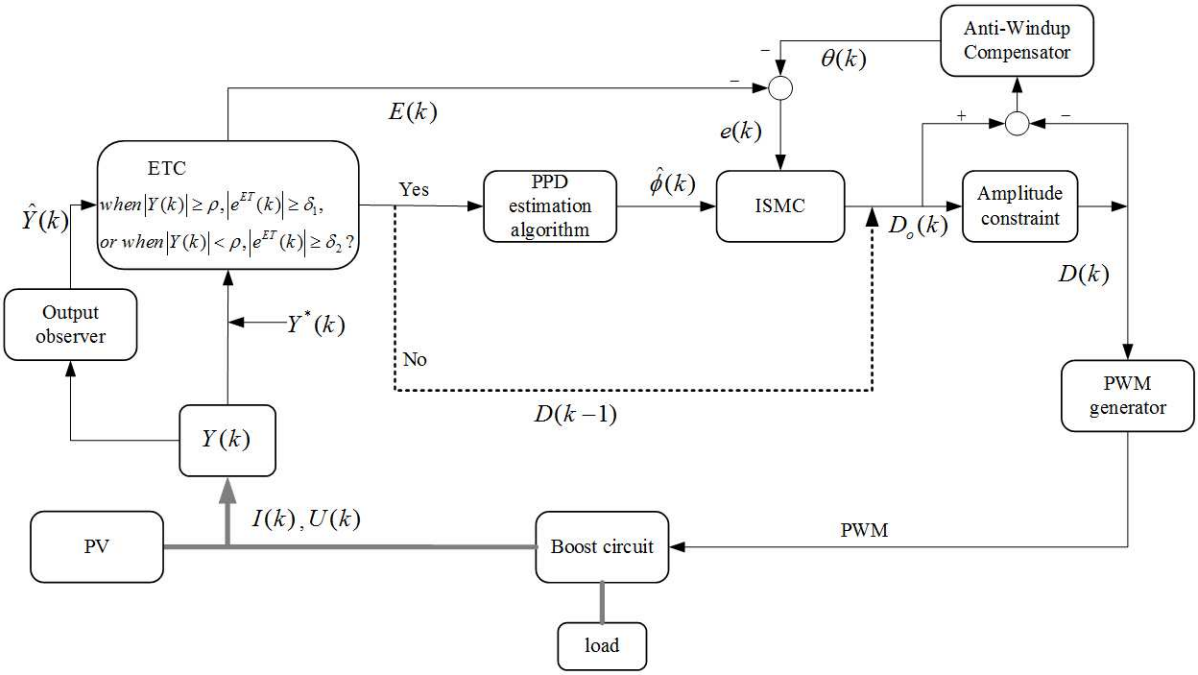


FIGURE 2. Block diagram of MFAC control strategy based on event triggering

By combining Equations (14), (15), (18), (19), and (22), we can obtain

$$\begin{aligned}
&\Delta s(k+1)\\
&= s(k+1) - s(k)\\
&= (1+\lambda T_s)e(k+1) - e(k)\\
&= (1+\lambda T_s)\left[Y^*(k+1) - Y(k+1) - \theta(k+1)\right] - e(k)\\
&= (1+\lambda T_s)\Bigg[Y^*(k+1) - \Big(\hat{Y}(k) + \hat{\phi}(k)\Delta D(k) + (2+G_o)e_o(k) - e_o(k-1)\Big)\\
&\quad - \Big(\eta\theta(k) + \hat{\phi}(k)(D_o(k) - D(k))\Big) - \frac{e(k)}{1+\lambda T_s}\Bigg]\\
&= (1+\lambda T_s)\Bigg[Y^*(k+1) - \hat{Y}(k) - (2+G_o)e_o(k) + e_o(k-1) - \eta\theta(k)\\
&\quad - \hat{\phi}(k)(D_{eq}(k) + D_{sw}(k)) - \frac{e(k)}{1+\lambda T_s}\Bigg]
\end{aligned} \tag{30}$$

Continuing with Equations (20) and (21), we can obtain

$$\begin{aligned}
\Delta s(k+1) &= -\mu s(k) + \frac{\varepsilon(1+\lambda T_s)}{\hat{\phi}^2(k)+\varepsilon}\left[\frac{\mu s(k)}{1+\lambda T_s} - \frac{\hat{\phi}^2(k)\upsilon \mathrm{sign}(s(k))}{\varepsilon(1+\lambda T_s)} + Y^*(k+1)\right.\\
&\quad \left. - \hat{Y}(k) - (2+G_o)e_o(k) + e_o(k-1) - \eta\theta(k) - \frac{e(k)}{1+\lambda T_s}\right]\\
&= -\mu s(k) + \frac{\varepsilon(1+\lambda T_s)}{\hat{\phi}^2(k)+\varepsilon}a(k)
\end{aligned} \tag{31}$$

where $a(k) = \frac{\mu s(k)}{1+\lambda T_s} - \frac{\hat{\phi}^2(k)\upsilon \text{sign}(s(k))}{\varepsilon(1+\lambda T_s)} + Y^*(k+1) - \hat{Y}(k) - (2+G_o)e_o(k) + e_o(k-1) - \eta\theta(k) - \frac{e(k)}{1+\lambda T_s}$.

At this point, we can obtain

$$\begin{aligned}\Delta V(k+1) &= \left(\frac{1}{2}\upsilon^2 - \upsilon\right)s^2(k) + \frac{\varepsilon(1-\upsilon)(1+\lambda T_s)a(k)}{\hat{\phi}^2(k)+\varepsilon}s(k) + \frac{\varepsilon^2(1+\lambda T_s)^2a^2(k)}{2\left(\hat{\phi}^2(k)+\varepsilon\right)^2} \\ &\leq a_0 s^2(k) + a_1 s(k) + a_2 \end{aligned} \tag{32}$$

where $\left(\frac{1}{2}\upsilon^2 - \upsilon\right) \leq a_0 < 0$, $a_1 = \frac{\varepsilon(1-\upsilon)(1+\lambda T_s)a(k)}{\hat{\phi}^2(k)+\varepsilon}s(k)$, $a_2(k) = \frac{\varepsilon^2(1+\lambda T_s)^2a^2(k)}{2\left(\hat{\phi}^2(k)+\varepsilon\right)^2}$.

For Equation (32), when $s(k) > \left(a_1 + \sqrt{a_1^2 + 4a_0a_2}\right) \Big/ (2a_0)$, $\Delta V(k+1) < 0$ can be obtained, which is $\lim_{k\to\infty}|s(k)| \leq \left(a_1 + \sqrt{a_1^2 + 4a_0a_2}\right) \Big/ (2a_0)$. According to [20], it can be obtained that

$$\lim_{k\to\infty}|e(k)| \leq \frac{\left(a_1 + \sqrt{a_1^2 + 4a_0a_2}\right)}{a_0\lambda T_s} \tag{33}$$

Therefore, when the values of $\lambda$ and $\varepsilon$ are appropriate, the system output tracking error satisfies the final consensus boundedness.

The stability of the model-free adaptive sliding mode constrained MPPT controller under event triggering can be discussed separately for event triggering and non-triggering. By selecting appropriate parameters, the output tracking error $e(k)$ of the system can be ensured to converge at all times $k$. The above demonstrated system is stable at all $k$ moments when the controller is working, and $k = k_i$ is a partial working time of the controller when the event is triggered. Therefore, the photovoltaic system is stable at $k = k_i$ moments when the event is triggered.

Therefore, the next step is to continue demonstrating the stability of the photovoltaic system before the event is triggered.

Assuming that the current time $\kappa$ is the time when any event has not been triggered and is between two adjacent triggering times, i.e., $\kappa \in (k_i, k_{i+1})$. So as the system runs, $k_i \to \infty$, then $\kappa \to \infty$. Based on the designed event triggering mechanism, it can be concluded that

$$\begin{aligned} e(\kappa+1) &= Y^*(\kappa+1) - Y(\kappa+1) - \theta(\kappa+1) \\ &= Y^*(\kappa+1) - (Y(\kappa) + (1+G_o)e_o(\kappa) - e_o(\kappa-1)) - \eta\theta(\kappa) \\ &= Y^*(\kappa+1) - \left(e^{ET}(\kappa) + Y(k_i) + Y^*(\kappa) - Y^*(k_i)\right) - \Theta(\kappa) \\ &= e(k_i) - e^{ET}(\kappa) + \Upsilon^*(\kappa) - \Theta(\kappa) \end{aligned} \tag{34}$$

where $\Upsilon^*(\kappa) = Y^*(\kappa+1) - Y^*(k_i)$, $\Theta(\kappa) = (1+G_o)e_o(\kappa) - e_o(\kappa-1) + \eta\theta(\kappa) - \theta(k_i)$.

In this article, the default given system output reference tracking signal $Y^*(k)$ is bounded, i.e., $Y_m^* \leq Y^*(k) \leq Y_M^*$. For $\Upsilon^*(\kappa)$, the following relationship can be obtained:

$$|\Upsilon^*(\kappa)| = |Y^*(\kappa+1) - Y^*(\kappa) + Y^*(\kappa) - Y^*(k_i)| \leq 2(Y_M^* - Y_m^*) = \Upsilon_m^* \tag{35}$$

Considering also that at the moment when the event is not triggered, the event triggering error $e^{ET}(k)$ satisfies $\left|e^{ET}(k)\right| < \delta$. Therefore, the following inequality can be derived from Equation (34):

$$\begin{aligned} |e(\kappa+1)| &\leq |e(k_i)| + \left|e^{ET}(\kappa)\right| + |\Upsilon^*(\kappa)| + |\Theta(\kappa)| \\ &< |e(k_i)| + \delta + \Upsilon_m^* + |\Theta(\kappa)| \end{aligned} \tag{36}$$

When the event is triggered, $\lim_{k_i\to\infty}|e(k_i)| = 0$, and when $k_i \to \infty$, $\kappa \to \infty$, so $\lim_{\kappa\to\infty}|e(k_i)| = 0$. According to [10], it is known that $\Theta(\kappa)$ also satisfies the final consensus boundedness, i.e., $\lim_{\kappa\to\infty}|\Theta(\kappa)| = 0$. Therefore, based on the above equation, the following relationship can be derived:

$$\lim_{\kappa\to\infty}|e(\kappa)| = \lim_{\kappa\to\infty}|e(\kappa+1)| < \left(\lim_{\kappa\to\infty}|e(k_i)| + \delta + \Upsilon_m^* + \lim_{\kappa\to\infty}|\Theta(\kappa)|\right) = \zeta \tag{37}$$

where $\zeta = \delta + \Upsilon_m^*$ is a positive real number.

Based on the above analysis, it can be concluded that as the system operates, the system output error corresponding to all events that have not been triggered will only fluctuate between intervals $(-\zeta, \zeta)$, indicating that the output error at this time is oscillating and converging.

Ultimately, it can be concluded that the proposed method remains stable even after incorporating event triggering.

4. **Simulation Analysis.** Firstly, photovoltaic cells and boost circuits are built in Simulink, and the proposed model-free adaptive integral sliding mode constrained MPPT control strategy is simulated and compared with traditional control methods.

Set the reference signal $Y^* = 0$ for the system output based on the condition that the photovoltaic cell operates at its maximum power point. To simulate changes in the external environment, the variations in light intensity S and temperature T are given as shown in Figure 3.

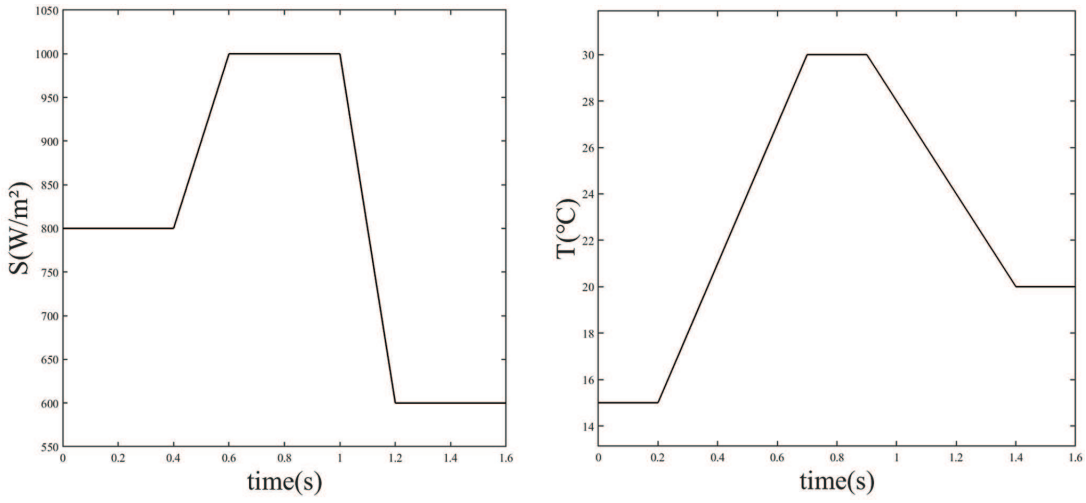


(a) (b)

FIGURE 3. Curve of changes in external environmental parameters of photovoltaic cells

Based on the theoretical analysis in the above section, the parameters in the controller have been selected with appropriate values within their respective ranges, as shown in Table 1.

Simulate under the above parameter conditions and obtain the simulation results shown in Figures 4 to 7. Figure 4 shows the output power of photovoltaic cells under different MPPT control methods. It can be seen from this that under the proposed model-free adaptive integral sliding mode constrained MPPT control strategy, the output power of the photovoltaic cell can quickly and accurately track the ideal reference maximum output power, and has strong stability under external environmental changes. In addition, to

TABLE 1. Values of various parameters in the controller

| Parameter | Value |
|---|---|
| $G_o$ | 0.9 |
| $\beta$ | 200 |
| $\sigma$ | $10^{-8}$ |
| $\hat{\phi}(1)$ | 0.005 |
| $D_{\min}$ | 0 |
| $D_{\max}$ | 1 |
| $\lambda$ | $5 \times 10^6$ |
| $\eta$ | 0.99 |
| $\varepsilon$ | $10^{-4}$ |
| $\upsilon$ | 0.05 |
| $\mu$ | $10^{-4}$ |
| $T_s$ | $10^{-6}$ |

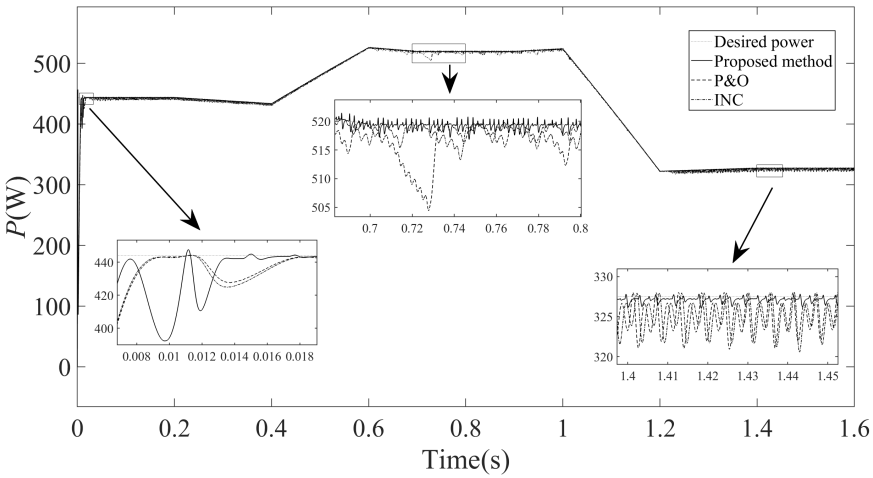


FIGURE 4. Output power of photovoltaic cells under different MPPT control methods

demonstrate the advantages of the control strategy proposed in this article, simulations are conducted using both P&O and INC methods under the same external conditions. In order to control the simulation variables, both methods have a step size of 0.05 V, and the output power curves are presented together in Figure 4.

From Figure 4, it can be seen that in terms of tracking time, the method proposed in this paper achieves stable tracking of maximum power in about 0.013 s, while the INC and P&O methods have slower tracking speeds, taking about 0.018 s. Therefore, the proposed method is slightly better than the other two methods in terms of tracking speed.

In the detailed enlarged view of 1.4-1.45 s in Figure 4, with a deviation of less than 0.5 w from the ideal reference maximum output power, the relative overall power output is almost negligible, and the tracking accuracy is extremely high. The deviation of the other two methods can reach 30000, which is 6-7 times that of the proposed method, and the tracking accuracy is inferior to the proposed method.

From Figure 4, it can also be seen that throughout the entire simulation time of 1.6 seconds, although the external light intensity and temperature are constantly changing, the

power output using the proposed method did not show any significant fluctuations overall, only an average fluctuation of 2 w up and down, with a fluctuation rate of about 0.4%, indicating extremely strong stability. On the other hand, the other two methods have significant fluctuations during tracking; for example, within the time period of 1.3-1.5 s, the fluctuation amplitude can reach two to three times that of the proposed method. Especially with the P&O method, there is a significant fluctuation between 0.7-0.75 s. Thus, the proposed method is also superior to the other two control methods in terms of control stability.

Figure 5 shows the variation curve of the duty cycle $D(k)$ of the proposed method. It can be seen that the value of $D(k)$ is always within $[0, 1]$, and the designed limiting constraint plays a role. Figure 6 shows the estimated PPD value, i.e., the variation of $\hat{\phi}(k)$. It can be seen that the variation of $\hat{\phi}(k)$ satisfies the reset mechanism set in this paper, thereby ensuring the controller's ability to track time-varying parameters.

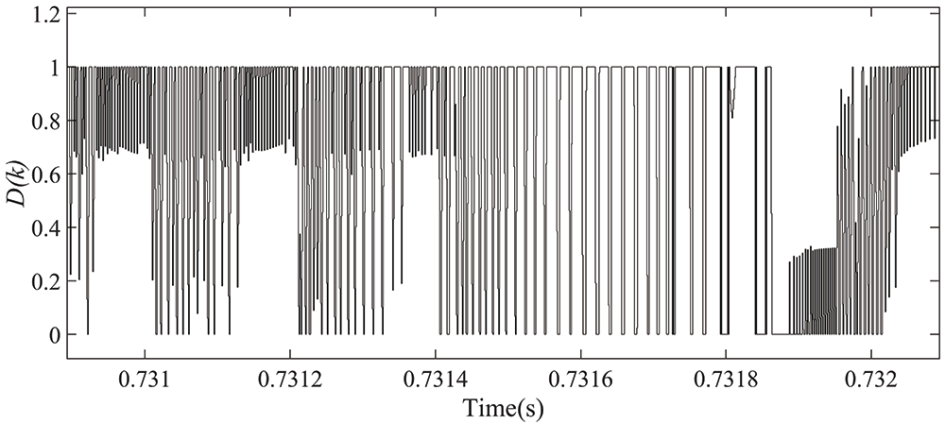


FIGURE 5. Duty cycle variation curve

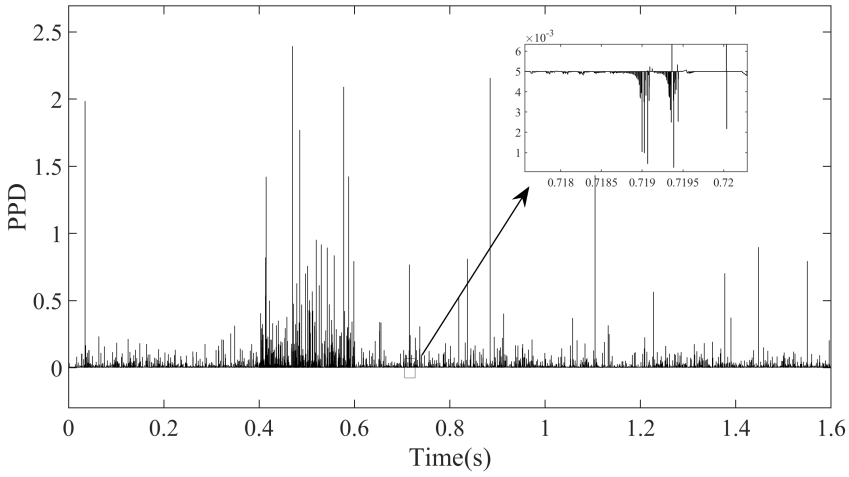


FIGURE 6. Pseudo partial derivative variation curve

Figure 7 shows the variation curve of the compensation signal $\theta(k)$ emitted by the anti-windup compensator. When $D(k)$ is constrained by amplitude limiting, $\theta(k)$ will immediately respond and make compensation to avoid saturation phenomenon. The above detailed analysis demonstrates that the simulation results obtained are consistent with the proposed theory, which further demonstrates the superior performance of the MPPT control strategy proposed in this paper in photovoltaic systems.

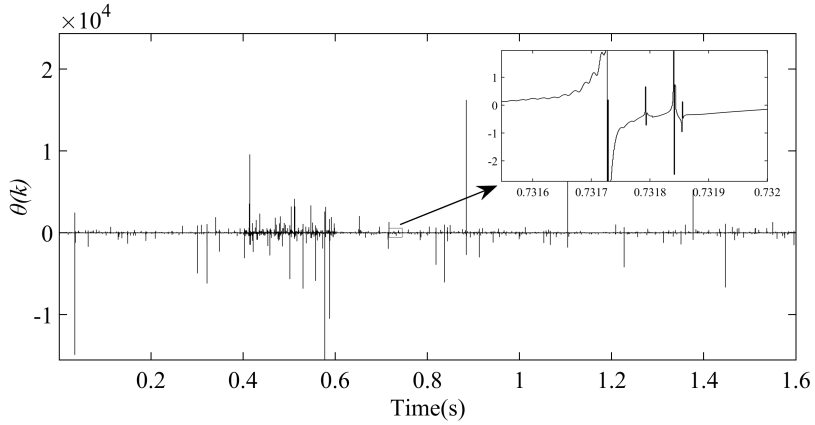


FIGURE 7. Compensation signal variation curve

In order to investigate the impact of event triggering on the tracking performance of the controller, four different sets of event triggering parameter values are set as shown in Table 2, including a control group without event triggering, for simulation comparison. The parameters of the controller and external environment parameters, except for the event triggering parameters, are consistent with the above experiment. In Table 2, $\delta_1$ and $\delta_2$ are the event triggering error thresholds $\delta$ when the second layer event is not triggered and triggered, respectively. When studying the impact of event triggering error thresholds, only one of $\delta_1$ and $\delta_2$ needs to be changed while keeping the other unchanged. The simulation results are shown in Figures 8 to 10 and Table 3.

TABLE 2. Event triggering parameter value table

| Group | Event triggering parameters |
|---|---|
| 1 | $\rho = 0.08$, $\delta_1 = 0.0002$, $\delta_2 = 0.0030$ |
| 2 | $\rho = 0.08$, $\delta_1 = 0.0002$, $\delta_2 = 0.0015$ |
| 3 | $\rho = 0.2$, $\delta_1 = 0.0002$, $\delta_2 = 0.0015$ |
| 4 | No event-triggered control |

Figure 8 shows the power tracking curves under different event triggering parameters. According to Figure 8, comparing groups 1, 2, and 4, it can be seen that as $\delta$ increases, power fluctuations also increase, and tracking accuracy and stability will weaken. By

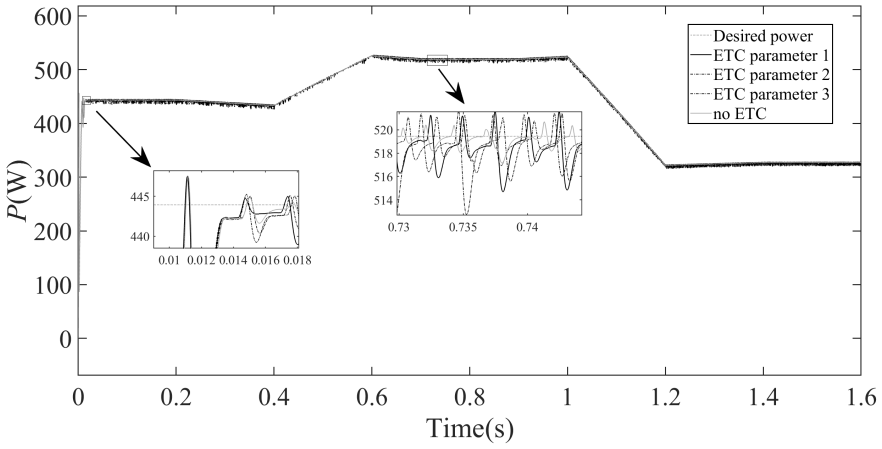


FIGURE 8. Output power under different event triggering parameters

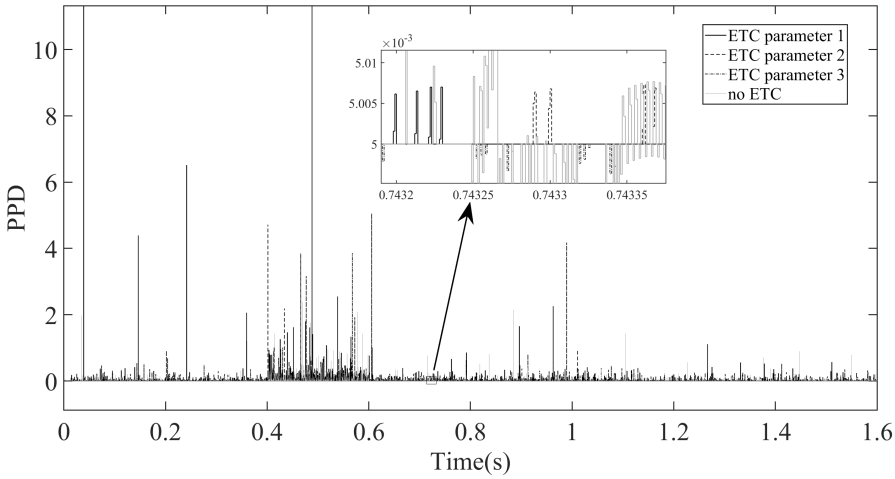


FIGURE 9. Pseudo partial derivative variation curve under different event triggering parameters

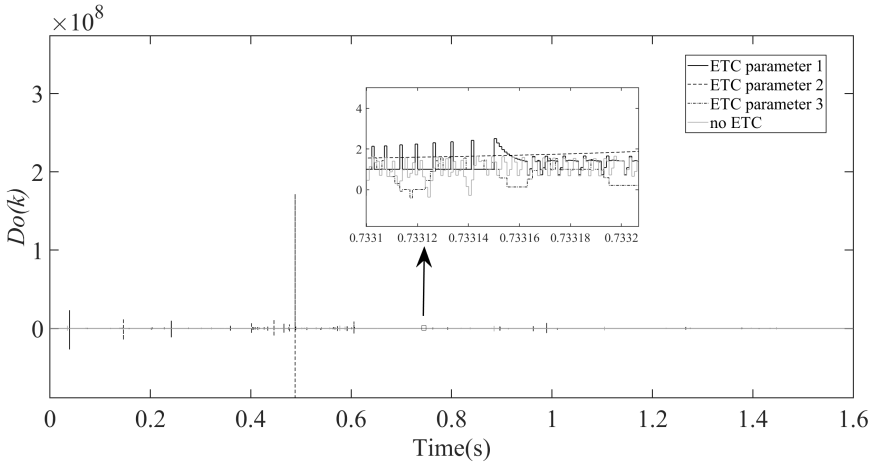


FIGURE 10. $D_o(k)$ variation curve

comparing the second, third, and fourth groups, it can be seen that as $\rho$ increases, power fluctuations also increase, and tracking accuracy and stability also weaken. Figure 9 shows the curve of pseudo partial derivative variation. It can be seen that as $\delta$ and $\rho$ increase, the number of PPD updates also decreases. Considering the existence of amplitude limiting effect, observing the change in $D(k)$ cannot accurately determine whether the integral sliding mode controller has updated the output. Therefore, Figure 10 shows the variation curve of $D_o(k)$ before the $D(k)$ limiting constraint. From Figure 10, it can be seen that as $\delta$ and $\rho$ increase, the number of updates for $D_o(k)$ decreases, which indirectly reflects the update situation of $D(k)$.

Table 3 shows the specific triggering times corresponding to each parameter group, with a total of $1.6 \times 10^6$ time points set in this simulation. It can be seen that, except for the control group which triggers updates at every moment, the other three groups have varying degrees of reduction in the number of triggers. And as $\delta$ and $\rho$ increase, the number of triggers also decreases.

Taking account of the results of this simulation, the following conclusion can be drawn: as $\delta$ and $\rho$ increase, the tracking performance of the system will decrease, and the reduction in controller computation will also be greater. Taking the second group with

TABLE 3. Triggering times corresponding to different event parameters

| Group | Number of event triggers |
|---|---|
| 1 | 990988 |
| 2 | 1079730 |
| 3 | 890885 |
| 4 | 1600000 |

relatively good performance as an example, the fluctuation is about twice that of not applying event-triggered control, but the triggering frequency is only 67.5% of the original, saving about one-third of the computational cost. Therefore, by adjusting the event triggering parameters, a balance between control performance and computational cost can be achieved.

5. **Conclusions.** In this paper, a model-free adaptive MPPT control strategy for photovoltaic systems is introduced. On the one hand, a nonlinear relationship model between the output and input of the photovoltaic system has been established by combining the principles of photovoltaic cells and the Boost circuit of the photovoltaic system. A linearized data-driven model of photovoltaic system is constructed using CFDL technology and observer-based PPD estimation algorithm, which solves the complex modeling problem of photovoltaic system. Meanwhile, the saturation problem of the actuator is solved by adding an anti-windup compensator. Besides, integral sliding mode control is introduced to improve system stability. And the proposed control method has been verified through simulation to have good tracking performance in MPPT control of the photovoltaic system. On the other hand, the proposed MPPT control method is combined with event triggering. The effectiveness of the proposed ETC strategy is verified through simulation. Although the event-triggered control strategy sacrifices some tracking performance, it greatly reduces the computational burden of the controller. By adjusting the event triggering parameters, it is possible to balance control performance and computational cost by adjusting the number of controller operations while ensuring the desired control performance.

In the future work, we will extend the researched event-triggered model-free adaptive integral sliding mode constrained maximum power point tracking control strategy for photovoltaic system to the photovoltaic storage integrated inverter system.

**Acknowledgment.** This work is partially supported by the National Natural Science Foundation of China (61973140). The authors also appreciatively acknowledge the helpful suggestions and comments of the reviewers, which have enhanced the presentation.

## REFERENCES

[1] B. Olfa, MPPT techniques for photovoltaic systems: A systematic review in current trends and recent advances in artificial intelligence, *Discover Energy*, vol.3, no.1, 2023.

[2] B. R. Babu, M. Suresh and B. P. Kumar, Hybrid, optimal, intelligent and classical PV MPPT techniques: A review, *CSEE Journal of Power and Energy Systems*, vol.7, no.1, pp.9-33, 2021.

[3] N. F. Ibrahim, M. M. Mahmoud, H. Alnami, D. E. M. Wapet, S. A. E. M. Ardjoun, M. I. Mosaad, A. M. Hassan and H. Abdelfattah, A new adaptive MPPT technique using an improved INC algorithm supported by fuzzy self-tuning controller for a grid-linked photovoltaic system, *PLoS One*, vol.18, no.11, 2023.

[4] A. Harrison, J. de Dieu Nguimfack-Ndongmo, N. H. Alombah, C. V. A. Kazé, R. Kuate-Fochie, D. A. Asoh and E. M. Nfah, Robust nonlinear MPPT controller for PV energy systems using PSO-based integral backstepping and artificial neural network techniques, *International Journal of Dynamics and Control*, pp.1598-1615, 2024.

[5] R. I. Areola, O. A. Aluko and O. I. Dare-Adeniran, Modelling of Adaptive Neuro-Fuzzy Inference System (ANFIS)-based Maximum Power Point Tracking (MPPT) controller for a solar photovoltaic system, *Journal of Engineering Research and Reports*, vol.25, no.9, pp.57-69, 2023.

[6] V. K. Dunna, K. P. B. Chandra, P. K. Rout, B. K. Sahu, P. Manoharan, A. R. Alsoud and B. Derebew, Super-twisting MPPT control for grid-connected PV/battery system using higher order sliding mode observer, *Scientific Reports*, 2024.

[7] H. Bhati and L. Gidwani, Real-time weather data analysis by the solar fuzzy logic-based MPPT controller, *Proc. of the Indian National Science Academy*, pp.924-940, 2023.

[8] S. M. A. Bakar, Z. Dongya, R. A. Ur, O. Khmeis and H. Habib, An adapted model predictive control MPPT for validation of optimum GMPP tracking under partial shading conditions, *Scientific Reports*, vol.14, no.1, 9462, 2024.

[9] S. R. D. Naoussi, K. T. Saatong, R. J. J. Molu, W. F. Mbasso, M. Bajaj, M. Louzazni, M. Berhanu and S. Kamel, Enhancing MPPT performance for partially shaded photovoltaic arrays through backstepping control with genetic algorithm-optimized gains, *Scientific Reports*, vol.14, no.1, 3334, 2024.

[10] C. Gao, W. Zhang, D. Xu, W. Yang and T. Pan, Event-triggered based model-free adaptive sliding mode constrained control for nonlinear discrete-time systems, *International Journal of Innovative Computing, Information and Control*, vol.18, no.2, pp.525-536, 2022.

[11] D. Xu, B. Jiang and F. Liu, Improved data driven model free adaptive constrained control for a solid oxide fuel cell, *IET Control Theory & Applications*, vol.10, no.12, pp.1412-1419, 2016.

[12] Z. Hou and S. Jin, Data-driven model-free adaptive control for a class of MIMO nonlinear discrete-time systems, *IEEE Transactions on Neural Networks/a Publication of the IEEE Neural Networks Council*, vol.22, no.12, pp.2173-2188, 2011.

[13] K. E. Åarzén, A simple event-based PID controller, *IFAC Proceedings Volumes*, vol.32, no.2, pp.8687-8692, 1999.

[14] P. Zhu, S. Jin, X. Bu and Z. Hou, Improved model-free adaptive control for MIMO nonlinear systems with event-triggered transmission scheme and quantization, *IEEE Transactions on Cybernetics*, vol.53, no.9, pp.5867-5880, 2023.

[15] M. Qi, P. Liu and Z. Zhao, Event-triggered adaptive sliding mode control for robotic manipulators with disturbance compensation, *Journal of the Brazilian Society of Mechanical Sciences and Engineering*, 2022.

[16] E. S. Abd, M. A. Hussien, M. Hamdy and T. A. Mahmoud, Event-triggered model-free adaptive control for nonlinear systems using intuitionistic fuzzy neural network: Simulation and experimental validation, *Complex & Intelligent Systems*, vol.10, no.2, pp.2271-2297, 2023.

[17] Q. Wang, S. Jin and Z. Hou, Event-triggered cooperative model-free adaptive iterative learning control for multiple subway trains with actuator faults, *IEEE Transactions on Cybernetics*, vol.53, no.9, pp.6041-6052, 2023.

[18] J. Zhou, Z. Yu, Z. Lu, C. Li and R. Zhang, Study of photovoltaic cells engineering mathematical model, *IOP Conference Series: Materials Science and Engineering*, vol.157, no.1, 2016.

[19] A. Youssef, M. M. Hefny and A. I. M. Ali, Investigation of single and multiple MPPT structures of solar PV-system under partial shading conditions considering direct duty-cycle controller, *Scientific Reports*, 2023.

[20] D. Xu, Y. Shi and Z. Ji, Model-free adaptive discrete-time integral sliding-mode-constrained-control for autonomous 4WMV parking systems, *IEEE Transactions on Industrial Electronics*, vol.65, no.1, pp.834-843, 2018.

## Author Biography

**Zhenchao Han** obtained a bachelor's degree in Electrical Engineering and Automation from Jiangnan University in 2022. He is currently pursuing a master's degree in Electrical Engineering at Jiangnan University in Wuxi, China.

His current research interests include photovoltaics and grid connected systems, maximum power tracking algorithms, etc.

**Tinglong Pan** obtained a doctoral degree in Power Electronics and Power Transmission from China University of Mining and Technology in 2004, Visited the University of Miami in the United States from June 2008 to June 2009, and worked as a postdoctoral fellow at the doctoral mobile station of Control Science and Engineering at Jiangnan University from October 2008 to October 2011.

Dr. Pan is currently a professor at the School of Internet of Things Engineering, Jiangnan University. His main research areas include microgrid control technology, power conversion technology and applications, electrical transmission systems and advanced control technology. He has presided over more than 10 longitudinal projects such as the National Natural Science Foundation and the National Postdoctoral Special Fund, and published over 100 academic papers.

**Dezhi Xu** obtained his Ph.D. degree from Nanjing University of Aeronautics and Astronautics in 2013 and currently serves as a professor at the School of Electrical Engineering, Southeast University in China.

Dr. Xu's research focuses on energy storage systems, motion and motor control, fault diagnosis and fault tolerance. He is a recipient of the National Excellent Youth Science Foundation of China and an IEEE Senior Member. He has led numerous national and provincial level projects, including the National Excellent Youth Science Foundation, National Natural Science Foundation General/Youth, and Joint Fund of the Ministry of Education, and published over 100 academic papers, including more than 60 SCI indexed papers.